

FoundIR-v2: Optimizing Pre-Training Data Mixtures for Image Restoration Foundation Model

Xiang Chen¹ Jinshan Pan¹ Jiangxin Dong¹ Jian Yang¹ Jinhui Tang²
¹ Nanjing University of Science and Technology ² Nanjing Forestry University
<https://lowlevelcv.com/>

Abstract

Recent studies have witnessed significant advances in image restoration foundation models driven by improvements in the scale and quality of pre-training data. In this work, we find that the data mixture proportions from different restoration tasks are also a critical factor directly determining the overall performance of all-in-one image restoration models. To this end, we propose a high-capacity diffusion-based image restoration foundation model, FoundIR-v2, which adopts a data equilibrium scheduling paradigm to dynamically optimize the proportions of mixed training datasets from different tasks. By leveraging the data mixing law, our method ensures a balanced dataset composition, enabling the model to achieve consistent generalization and comprehensive performance across diverse tasks. Furthermore, we introduce an effective Mixture-of-Experts (MoE)-driven scheduler into generative pre-training to flexibly allocate task-adaptive diffusion priors for each restoration task, accounting for the distinct degradation forms and levels exhibited by different tasks. Extensive experiments demonstrate that our method can address over 50 sub-tasks across a broader scope of real-world scenarios and achieves favorable performance against state-of-the-art approaches.

1. Introduction

Recent years have witnessed significant progress in the development of foundation models, which are pre-trained on large-scale data and applied across a wide range of downstream tasks [26, 53]. Inspired by this popular trend, image restoration foundation models have attracted increasing attention, aiming to simultaneously address extensive restoration tasks within a universal model.

In practice, the efficacy of image restoration foundation models is governed by two critical factors: the composition of training data and the choice of the base model. The former determines the scope of tasks that the model can learn, whereas the latter dictates its overall learning capability. To-

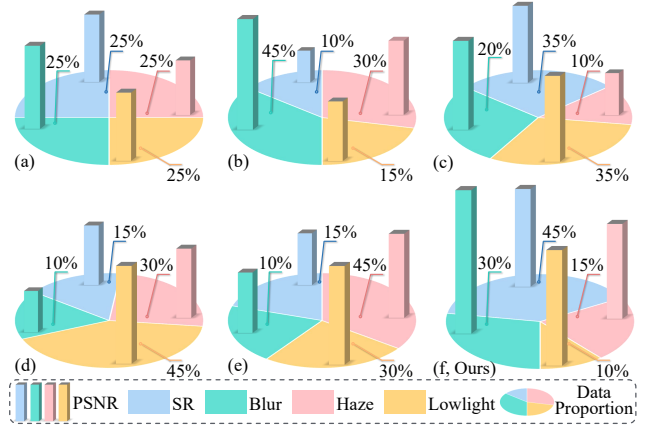


Figure 1. Statistical analysis of the relationship between data mixture proportions and restoration performance for all-in-one foundation model. To facilitate clearer observations, we restrict the experimental analysis to four tasks: deblurring, dehazing, low-light enhancement, and SR. In the figure, the pie chart illustrates the training data distribution across different tasks, while the bar chart reports the corresponding PSNR results on each task’s test set.

gether, these two factors jointly influence the comprehensive performance and robustness of the foundation model.

With respect to **training data**, existing studies primarily focus on scaling up datasets via data synthesis [42] and real-world collection [26] to advance the performance upper bound of universal image restoration. However, limited attention has been paid to the intricate relationship between the compositional proportions of mixed training datasets (*i.e.*, the relative data volume allocated to different restoration tasks) and the resulting all-in-one restoration capabilities of foundation models. In fact, the composition of training data from different tasks in a foundation model naturally differs. In addition, inter-task data interactions during training can exhibit complex relationships that can be facilitative, independent, or even conflicting [5]. We observe that employing equal or random sampling ratios from different task-specific datasets often leads to considerable performance instability in all-in-one restoration models (see Figure 1). In other words, an inappropriate mixture ratio may

result in inefficient training or inadequate learning for foundation models. These insights motivate us to systematically optimize the data composition, with the goal of balancing foundation model capabilities across tasks while leveraging potential synergies among them.

Regarding the **base framework**, recent diffusion-based approaches have emerged as promising candidates for image restoration foundation model, due to their powerful generative priors that enhance model generalization [34]. However, existing approaches usually either use diffusion models directly [26, 35, 64] or fine-tune pretrained ones for all restoration tasks [29, 58], without adequately accounting for the task-dependent impact of diffusion priors under distinct reconstruction objectives. For example, when processing low-resolution hazy images, current all-in-one restoration methods only perform image dehazing, overlooking the necessity of concurrent super-resolution (SR). This oversight significantly constrains the potential of diffusion priors to achieve high-quality reconstruction. Thus, this motivates us to adaptively allocate task-specific diffusion priors, improving the joint optimization of various restoration capabilities under dynamic data mixing.

To address these issues, we propose FoundIR-v2, an effective image restoration foundation model capable of handling more than 50 subtasks. Building upon FoundIR [26], which investigates the effects of training **data scaling laws** in image restoration foundation models, this work further uncovers the **data mixing laws** that govern how mixture proportions influence all-in-one image restoration. Specifically, we introduce a flexible data equilibrium scheduling paradigm that dynamically adjusts the composition ratios within the training data pool. This approach enhances the efficacy of data distributions and strengthens the model’s all-in-one restoration ability, thereby catalyzing synergistic interactions across tasks. In contrast to the static sampling strategies used in existing approaches [26, 64], our dynamic data mixing scheme enables the model to obtain comprehensive restoration capabilities more rapidly during the early learning stages, rather than gradually converging at the final stage. Furthermore, we integrate a mixture-of-experts (MoE)-driven scheduler with Stable Diffusion (SD) to adaptively allocate useful generative priors tailored to the heterogeneous demands of different restoration tasks. Note that we jointly optimize both data and model scheduling schemes, enabling our method to better align dynamic data mixtures with adaptive model capabilities during generative pre-training. Extensive experiments show that our FoundIR-v2 outperforms state-of-the-art models in a range of real-world scenarios and downstream applications.

We summarize our main contributions as follows:

- We propose FoundIR-v2, an up-to-date image restoration foundation model that dynamically optimizes pre-training data mixtures to better balance the model’s ca-

pabilities in all-in-one restoration tasks.

- We develop an effective MoE-driven diffusion scheduler to dynamically allocate diverse task-adaptive diffusion priors for each restoration tasks during the generative pre-training process.
- We demonstrate the effectiveness of the data mixing laws, and show that our FoundIR-v2 addresses over 50 sub-tasks across broader real-world scenarios, outperforming state-of-the-art approaches.

2. Related Work

Model scaling laws for image restoration. Recent studies on model scaling laws in LLMs [37] have demonstrated that increasing model parameters and computational resources leads to more powerful foundation models with improved generalization performance and enhanced reasoning capabilities. In image restoration, this perspective is being extended to explore effective architectures capable of handling a wide range of real-world degradation tasks within a unified foundation model [26]. Vision Transformers (ViT) have demonstrated strong potential due to their global receptive fields and scalable design, enabling deeper and wider models for low-level vision. For example, Chen *et al.* [7] propose a ViT-based pre-trained large model (IPT) for image processing using 32 NVIDIA Tesla V100 GPUs (32GB).

Recently, diffusion models [8] have emerged as a popular paradigm for image restoration by unleashing generative priors to help model generalization. SUPIR [58] scales up large diffusion models by leveraging a robust large-scale adapter to improve perceptual quality and use text prompts for real-world image restoration. Later, OmniLV [41] integrates advanced Diffusion Transformer (DiT)-based generative priors into a multimodal framework, advancing toward general low-level vision [11]. More recently, HYPIR [30], trained on 64 NVIDIA A6000 GPUs (48GB), leverages a pre-trained diffusion model for efficient parameter initialization and then applies lightweight adversarial fine-tuning to adapt it specifically for image restoration. In this paper, we train a robust image restoration foundation model on high-memory NVIDIA H20 GPUs (96 GB), leveraging the great potential of MOE-guided diffusion models.

Data scaling and mixing laws for image restoration. It is well-known that the training data for foundation models has a significant influence on their performance. Li *et al.* [26] find that as the size of real-world training data continues to grow, the performance of all-in-one image restoration models improves substantially. To this end, FoundIR is proposed by establishing a unified data collection system that enables the acquisition of a million-scale high-quality paired dataset to advance image restoration foundation models [26]. Furthermore, Rajagopalan *et al.* [42] introduce a diffusion-based degradation data synthesis approach that ensures diversity in training data, thereby en-

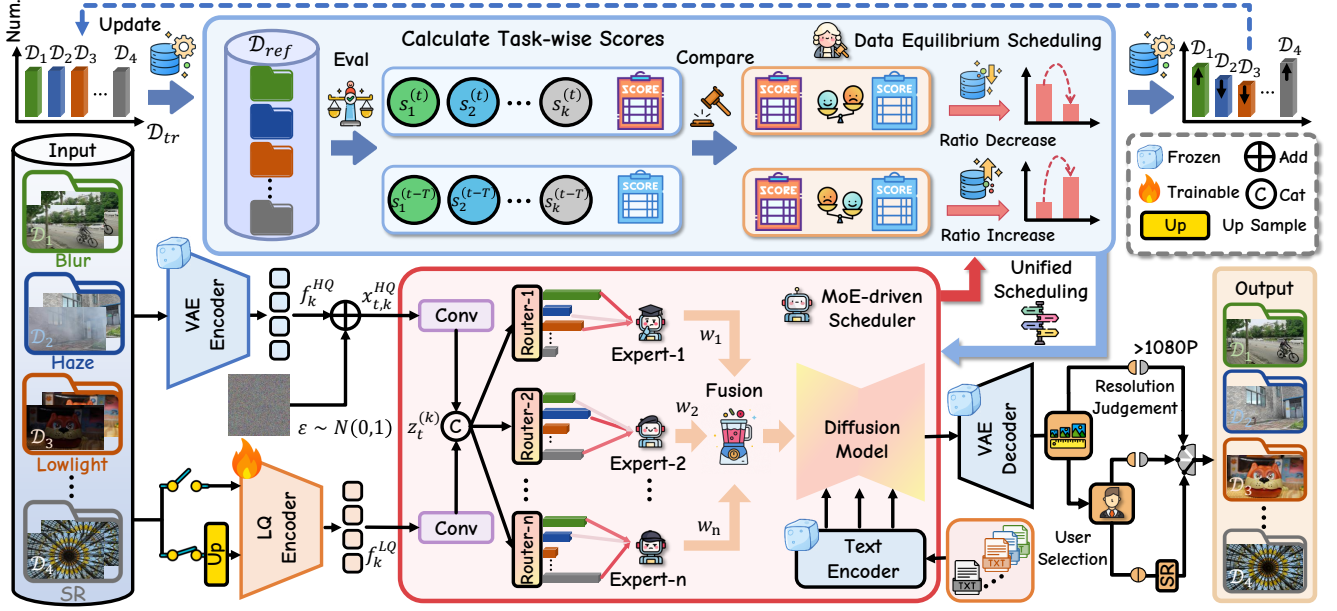


Figure 2. Illustration of the proposed FoundIR-v2. We adopt a dual scheduling strategy for both the training data and the base model, including (i) a data equilibrium scheduling is introduced into the pre-training process to dynamically optimize the data mixture, and (ii) an MoE-driven scheduler is integrated into the model to dynamically allocate task-adaptive diffusion priors. For low-resolution LQ inputs, our proposed FoundIR-v2 allows users to flexibly choose at test time whether to retain the original image resolution or apply SR operation.

hancing the generalization capability of universal image restoration models. We note that while existing studies focus on increasing the size and quality of training datasets, few works explore how the mixture proportions of different degradation data effect the performance for all-in-one image restoration. In fact, Data Mixing Law [37] introduces a mixing proportion principle derived from extensive experiments in the LLM era, revealing the relationship between data proportions and their corresponding tasks and providing guidance for adjusting data distributions. In this work, we fill this research gap and propose optimizing data mixtures to better train image restoration foundation models.

3. Proposed Method: FoundIR-v2

Our goal is to formulate an effective foundation model that can address a broader range of image restoration tasks. Towards this goal, we propose FoundIR-v2, which maximizes the effectiveness of mixed training datasets and model capacity. We propose a data equilibrium scheduling scheme and an MoE-driven diffusion scheduler, which are jointly optimized within a unified multi-task framework. In what follows, we present the details of the proposed approach.

3.1. Overall framework

As illustrated in Figure 2, our method utilizes a pre-trained Variational Autoencoder (VAE) [23] encoder to project low-quality (LQ) images into the latent space, producing latent representations denoted as f_k^{LQ} . Note that the SR task differs from other restoration tasks in that its LQ and HQ im-

ages have different image resolutions. To facilitate unified training for all tasks, for LQ inputs I_{LQ} originating from SR datasets, we apply a random upsampling operation from a set of interpolation techniques, including nearest-neighbor, bilinear, and bicubic interpolation, to align the spatial dimensions of SR inputs with the model’s output resolution.

For the base framework, we adopt the SDXL [39] backbone as our diffusion model, which is pre-trained on high-quality (HQ) images I_{HQ} to produce the corresponding latent features denoted as f_k^{HQ} . To better allocate appropriate diffusion priors from SD for each task, we integrate an effective MoE-driven scheduler with the SDXL-based generative pre-training for joint optimization. In addition, we employ LLaVA [31] to generate image descriptions for all training datasets. These text embeddings are integrated with the latent features via cross-attention layers to leverage auxiliary text-to-image information for better image restoration [8]. To ensure adequate task learning and prevent performance imbalance [26], we incorporate a data equilibrium scheduling scheme into the multi-task learning procedure. By performing iterative data mixture optimization, we obtain the final outputs using a pre-trained VAE decoder [23].

3.2. Data equilibrium scheduling

Problem formulation. Assume that a base model \mathcal{M}_0 with parameters $\theta \in \mathbb{R}^M$ is given. Our final objective is to build upon \mathcal{M}_0 to train an effective image restoration foundation model capable of handling diverse sub-tasks. For the large-scale training data \mathcal{D}_{tr} , we partition it into k categories ac-

cording to task attributes (*e.g.*, image enhancement, super-resolution), where each category is associated with a set of training dataset \mathcal{D}_i . Let N denote the total number of training samples, *i.e.*, $N = |\mathcal{D}_{tr}| = |\mathcal{D}_1| + \dots + |\mathcal{D}_k|$, where $|\mathcal{D}_i|$ represents the cardinality of the task-specific training dataset \mathcal{D}_i . When simply mixing data from multiple tasks, like $\mathcal{D}_{tr} = \mathcal{D}_1 \cup \dots \cup \mathcal{D}_k$, the foundation model tends to exhibit imbalanced capabilities due to the inappropriate training data distribution. To facilitate the optimization of training pool, we define the data mixture proportions (weights) λ as the sampling probability over the k domains, thereby specifying the distribution of training data:

$$P_\lambda = \sum_{i=1}^k \lambda_i \text{unif}(\mathcal{D}_i), \quad (1)$$

where $\text{unif}(\mathcal{D}) = \frac{1}{|\mathcal{D}|} \sum_{x \in \mathcal{D}} \delta_x$ is the uniform distribution over the image samples in \mathcal{D} , and δ_x denotes the Dirac delta function centered at sample x . Given a fixed model size, the training seeks to obtain the optimal model parameters θ^* by minimizing the L1-normalized function:

$$\theta_\lambda^* = \arg \min_{\theta} \|I_{HQ} - \mathcal{M}_0(I_{LQ})\|_1, \quad (2)$$

where $\|\cdot\|_1$ denotes the L1-normalized reconstruction loss.

Optimization of data mixture. We note that existing methods [26, 36, 64] typically adopt statically fixed data mixing ratios for model training. To maximize the effectiveness of mixed training dataset, we dynamically optimize the data mixture by redefining the ratios at scheduled intervals during the training iterations. Specifically, we first construct an initial training batch by uniformly sampling from the subsets $\{\mathcal{D}_1, \dots, \mathcal{D}_k\}$ of \mathcal{D}_{tr} . After every interval of T iterations, the performance of the current model is evaluated on a small independent reference dataset \mathcal{D}_{ref} to validate its multi-task restoration performance. Here, \mathcal{D}_{ref} is randomly sampled from \mathcal{D}_{tr} across k categories, with an equal number of samples per task, and it is disjoint from \mathcal{D}_{tr} . Based on this evaluation, we obtain task-wise performance scores $s_1^{(t)}, \dots, s_k^{(t)}$ at iteration t on \mathcal{D}_{ref} . To track multi-task restoration performance trends, we compare them with those at the previous checkpoint $s_1^{(t-T)}, \dots, s_k^{(t-T)}$. If the performance of task j degrades, *i.e.*, $s_j^{(t)} < s_j^{(t-T)}$, we increase its data sampling probability in the next training interval to allocate more supervision from \mathcal{D}_j . Conversely, if a task maintains or improves performance, its weight can be reduced slightly to balance the overall data distribution.

Formally, we define the rule for data optimization as

$$\lambda_j^{(t+1)} = \frac{\lambda_j^{(t)} \exp(-\alpha \Delta s_j^{(t)})}{\sum_{i=1}^k \lambda_i^{(t)} \exp(-\alpha \Delta s_i^{(t)})}, \quad (3)$$

where $\Delta s_j^{(t)} = s_j^{(t)} - s_j^{(t-T)}$ denotes the performance change of task j , and $\alpha > 0$ is a scaling factor controlling

Algorithm 1 Data Equilibrium Scheduling

Require: Initial model \mathcal{M}_0 , task categories k , training dataset $\mathcal{D}_{tr} = \{\mathcal{D}_{tr}^1, \dots, \mathcal{D}_{tr}^k\}$, reference dataset $\mathcal{D}_{ref} = \{\mathcal{D}_{ref}^1, \dots, \mathcal{D}_{ref}^k\}$, evaluation interval T , maximum iterations I , sample batches $\{\mathcal{D}_1, \dots, \mathcal{D}_k\}^t \in \mathcal{D}_{tr}$.

- 1: **for** $t = 1$ to I **do**
- 2: Train model \mathcal{M}_t on sample batches $\{\mathcal{D}_1, \dots, \mathcal{D}_k\}^t$;
- 3: **if** $t \bmod T = 0$ **then**
- 4: Evaluate \mathcal{M}_t on $\mathcal{D}_{ref} = \{\mathcal{D}_{ref}^1, \dots, \mathcal{D}_{ref}^k\}$ to obtain current scores $\{s_1^t, \dots, s_k^t\}$ for all tasks k ;
- 5: **for** $j = 1$ to k **do**
- 6: **if** $s_j^t < s_j^{(t-T)}$ **then**
- 7: Increase data sampling proportion $\lambda_j^{(t+T)}$;
- 8: **else**
- 9: Decrease data sampling proportion $\lambda_j^{(t+T)}$;
- 10: **end if**
- 11: **end for**
- 12: **end if**
- 13: Update sample batches $\{\mathcal{D}_1, \dots, \mathcal{D}_k\}^{(t+T)} \in \mathcal{D}_{tr}$;
- 14: **end for**
- 15: **return** Final model \mathcal{M}_I .

the sensitivity of composition proportion adjustment. This softmax-based normalization ensures $\sum_{j=1}^k \lambda_j^{(t+1)} = 1$, while reweighting the sampling probabilities across tasks.

The pseudocode for data equilibrium scheduling is presented in Algorithm 1. Through this dynamic optimization scheme, our method allocates more data to underperforming tasks while preventing overfitting on already well-learned tasks, thereby mitigating task imbalance and improving the overall generalization of the foundation model.

3.3. MoE-driven diffusion scheduler

Since diverse image restoration tasks involve heterogeneous reconstruction demands in multi-task learning, we integrate an MoE-driven scheduler into the generative pre-training to allocate task-adaptive diffusion priors. Specifically, given the LQ feature f^{LQ} and the noisy latent x_t^{HQ} from k tasks generated by the diffusion model at timestep t , we first obtain a fused representation $\mathbf{z}_t^{(k)} = \phi(f_k^{LQ}, x_{t,k}^{HQ})$, where $\phi(\cdot)$ denotes the concatenation operation. Then, this representation is fed into an MoE-driven scheduler consisting of n shared experts to capture diverse degradation patterns. By the router's dynamic selection, the associated weights $w_i^{(k)}$ generated by different experts are defined as follows:

$$w_i^{(k)} = \frac{\exp(\mathbf{g}_i^{(k)\top} \mathbf{z}_t^{(k)})}{\sum_{j=1}^n \exp(\mathbf{g}_j^{(k)\top} \mathbf{z}_t^{(k)})}, \quad (4)$$

where $\mathbf{g}_i^{(k)}$ is the learnable gating parameter for each expert. This formulation converts the scores of all experts into

non-negative weights that sum to 1, enabling a weighted combination of the outputs from all experts.

Here, each expert $E_i(\cdot)$ denotes a type of attention mechanism (e.g., spatial [45], channel [60], or sparse [9]), designed to activate different cues based on task requirements. By executing model scheduling, our method can effectively exploit useful information from the degraded inputs across different tasks, thereby facilitating the subsequent diffusion process. Finally, we obtain the scheduled feature representation $\mathcal{F}^{(k)}$, which is defined as follows:

$$\mathcal{F}^{(k)}(z_t) = \sum_{i=1}^n w_i^{(k)} E_i(z_t^{(k)}). \quad (5)$$

Inspired by [8], we first pre-train only the MoE-driven scheduler, and then jointly fine-tune the scheduler and the diffusion model, in order to better enhance the consistency of multi-task feature utilization for generative pre-training.

4. Experiments

4.1. Experimental settings

Training dataset. We combine publicly available datasets from a diverse set of image restoration tasks to form our training dataset [1, 6, 12, 14, 15, 17, 20, 26–28, 62]. We note that existing studies only focus on the quality of LQ images in the training dataset (*i.e.*, data diversity of different degradation types), but ignore the impact of GT image quality on all-in-one restoration performance. In other words, existing approaches simply combine the GT images from individual restoration tasks, while overlooking the common characteristics of clear images across all tasks. For example, Figure 3 shows a visual example from the dehazing task in the existing training set. Although its GT image is haze-free, it contains other visible degradation types, such as blur and noise. This would lead to negative conflicts in learning objectives during the data mixing training, potentially interfering with the model’s generalization performance.

To alleviate this problem, we employ recent multi-modal image quality assessment (IQA) models [36, 57] to perform degradation identification and quality evaluation on the GT images within the training dataset. By leveraging the IQA models, we further filter out low-quality GT samples, ensuring that only high-quality data are retained for training. This data cleaning process can mitigate potential data contamination effects during pre-training data mixture.

Test datasets. To comprehensively evaluate the generalization ability of our model in all-in-one image restoration, we test the model on a wide range of benchmark datasets across diverse tasks, *i.e.*, 4KRD [14], LSD [62], PolyU [52], HQ-NightRain [16], UAV-Rain1k [6], WeatherBench [17], Dense-HAZE [3], NH-HAZE [4], RS-Cloud [38], UHD-LL [25], FoundIR-TestData [26], RealPhoto60 [58], and RealDeg [8]. More experimental results on other restoration tasks are included in the supplementary material.

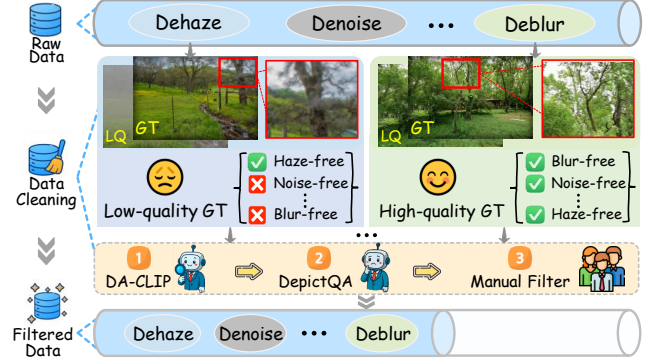


Figure 3. Visual example of high-quality GT data filtering.

Evaluation metrics. We evaluate the fidelity and quality of restored images using PSNR, SSIM, and a set of perceptual metrics (*i.e.*, LPIPS [63], MUSIQ [22], CLIPQA+ [47], PIQE [46], MANIQA [54] and PaQ-2-PiQ [56]).

Implementation details. We train our proposed FoundIR-v2 on two NVIDIA H20 GPUs (96 GB) using the AdamW optimizer [33] with default parameters. During training, images are randomly cropped into 512×512 patches, with a batch size of 32. We follow the unified feature optimization strategy in [8]. The initial learning rate of the VAE encoder is set to 5×10^{-6} , while that of the other components is set to 5×10^{-5} . The learning rate is subsequently scheduled by the cosine annealing scheme [32]. We train the network for a total of 150,000 iterations. During the validation, MUSIQ is employed to calculate task-wise scores for the SR task, whereas PSNR is used for other tasks. For \mathcal{D}_{ref} , the number of validation samples for each task category is 10. During the model inference, we adopt the Euler scheduler [21] with 20 sampling timesteps for all tasks, while the classifier-free guidance (CFG) [18] scale is fixed at 5. For the SR task, we employ AdaIN as the color-fix strategy, while no color-fix is applied to the other tasks. The code will be available.

4.2. Comparisons with the state of the art

Evaluation on the public benchmarks. We first evaluate our FoundIR-v2 on public benchmark datasets across different restoration tasks and report the quantitative results in Table 1. We compare our method with state-of-the-art restoration methods, including all-in-one image restoration approaches (*i.e.*, PromptIR [40], TransWeather [44], DA-CLIP [36], DiffUIR [64], AutoDIR [19], InstructIR [13], X-Restormer [10], FoundIR [26]), and real-world super-resolution (SR) approaches (*i.e.*, Real-ESRGAN [49], BSRGAN [61], StabSR [48], PASD [55], SeeSR [51], DreamClear [2], OSediff [50], SUPIR [58], FaithDiff [8]). Based on the statistics of five evaluation metrics on these test sets, our method achieves the best or second-best performance in more than 80% of the quantitative comparisons. Compared with existing all-in-one image restoration models, our FoundIR-v2 demonstrates more comprehensive restoration

Table 1. Quantitative comparisons with state-of-the-art general restoration methods, all-in-one restoration models, image restoration agent, and real-world SR approaches on benchmark datasets. **Red** and **Blue** indicate the best and the second-best performance.

Methods	4KRD (Motion Deblurring) [14]					LSD (Defocus Deblurring) [62]					PolyU (Denoising) [52]				
	PSNR ↑	SSIM ↑	LPIPS ↓	MUSIQ ↑	CLIPQA+ ↑	PSNR ↑	SSIM ↑	LPIPS ↓	MUSIQ ↑	CLIPQA+ ↑	MUSIQ ↑	CLIPQA+ ↑	PIQE ↓	MANIQA ↑	PaQ-2-PiQ ↑
PromptIR [40]	24.74	0.7678	0.3386	21.02	0.3232	19.63	0.7335	0.5582	15.04	0.2225	51.80	0.3873	60.3508	0.5182	68.7471
TransWeather [44]	23.36	0.7231	0.4384	17.78	0.2563	19.87	0.7308	0.5563	14.85	0.2468	32.99	0.3111	80.8918	0.4030	59.8569
DA-CLIP [36]	23.84	0.7347	0.4408	18.13	0.3103	19.65	0.7313	0.5179	15.73	0.2178	42.13	0.3547	74.2320	0.4774	65.3832
DiffUIR [64]	24.69	0.7596	0.3562	20.22	0.3225	19.71	0.7357	0.5818	16.05	0.2071	45.53	0.3561	73.2232	0.4611	66.6793
AutoDIR [19]	24.21	0.7288	0.4396	18.42	0.2917	20.01	0.7431	0.5163	18.82	0.2389	37.67	0.3538	80.3762	0.4496	63.2148
InstructIR [13]	26.28	0.8181	0.2307	27.84	0.3844	19.28	0.7227	0.5220	15.82	0.2121	52.14	0.4445	40.8439	0.5254	70.7628
X-Restormer [10]	24.57	0.7604	0.3823	19.97	0.3188	19.46	0.7336	0.5854	15.84	0.2288	32.99	0.3111	80.8918	0.4030	59.8569
AgenticIR [65]	24.41	0.7569	0.4021	18.73	0.3196	18.30	0.7146	0.5337	22.63	0.2608	35.98	0.3186	79.2196	0.4580	62.2334
FoundIR [26]	26.59	0.8188	0.2351	27.35	0.3676	19.18	0.7306	0.5701	15.92	0.2007	49.92	0.4244	42.0997	0.5293	70.9032
Ours	26.64	0.7997	0.1451	34.93	0.4796	20.78	0.6708	0.3658	50.74	0.3615	48.68	0.4276	31.7934	0.5497	70.2896
Methods	Dense-HAZE (Dehazing) [3]					NH-HAZE (Non-Homogeneous Dehazing) [4]					RS-Cloud (Declouding) [38]				
	PSNR ↑	SSIM ↑	LPIPS ↓	MUSIQ ↑	CLIPQA+ ↑	PSNR ↑	SSIM ↑	LPIPS ↓	MUSIQ ↑	CLIPQA+ ↑	PSNR ↑	SSIM ↑	LPIPS ↓	MUSIQ ↑	CLIPQA+ ↑
PromptIR [40]	9.57	0.4333	0.7889	26.16	0.2406	11.38	0.4343	0.6077	50.40	0.3288	11.35	0.7716	0.2713	41.83	0.4739
TransWeather [44]	10.51	0.4523	0.7900	27.85	0.2060	11.58	0.4110	0.6921	40.22	0.2543	12.93	0.7081	0.3808	30.02	0.3390
DA-CLIP [36]	10.94	0.4590	0.7604	30.07	0.2451	12.35	0.4662	0.5903	49.73	0.3364	16.43	0.8028	0.2383	35.73	0.4839
DiffUIR [64]	9.59	0.4326	0.7994	26.42	0.2680	11.39	0.4220	0.6508	47.77	0.3068	13.82	0.8140	0.2602	38.44	0.4210
AutoDIR [19]	12.33	0.4862	0.7364	31.97	0.2167	12.71	0.4774	0.6119	46.29	0.2991	18.39	0.8093	0.2519	31.44	0.4390
InstructIR [13]	11.03	0.4649	0.7456	32.96	0.1615	12.24	0.4984	0.5303	54.80	0.2455	14.46	0.8647	0.1624	47.00	0.3538
X-Restormer [10]	9.57	0.4295	0.8049	24.09	0.2486	11.36	0.4131	0.6653	44.28	0.2967	11.48	0.7506	0.3252	35.99	0.3641
AgenticIR [65]	10.11	0.3884	0.7960	27.73	0.2595	12.20	0.4495	0.6745	37.47	0.3664	17.80	0.7992	0.2572	34.90	0.4297
FoundIR [26]	9.29	0.4307	0.7951	27.80	0.2522	11.43	0.4491	0.5817	54.53	0.2978	11.71	0.7527	0.3219	35.40	0.4295
Ours	15.29	0.5063	0.4975	57.48	0.3672	17.00	0.4616	0.3338	62.62	0.4065	22.06	0.8278	0.1251	44.37	0.4411
Methods	HQ-NightRain (Deraining) [16]					UAV-Rain1k (Raindrop Removal) [6]					WeatherBench (Desnowing) [17]				
	PSNR ↑	SSIM ↑	LPIPS ↓	MUSIQ ↑	CLIPQA+ ↑	PSNR ↑	SSIM ↑	LPIPS ↓	MUSIQ ↑	CLIPQA+ ↑	PSNR ↑	SSIM ↑	LPIPS ↓	MUSIQ ↑	CLIPQA+ ↑
PromptIR [40]	10.43	0.4485	0.5684	38.70	0.3727	15.16	0.6605	0.4025	64.44	0.5712	21.54	0.7767	0.2421	45.20	0.3622
TransWeather [44]	12.88	0.4774	0.6642	28.58	0.2855	14.85	0.5381	0.5984	51.68	0.4145	20.94	0.7579	0.2531	44.25	0.3306
DA-CLIP [36]	14.78	0.5398	0.5717	32.11	0.3500	15.38	0.6035	0.4414	62.41	0.5867	21.59	0.7731	0.2357	45.22	0.3624
DiffUIR [64]	11.58	0.4827	0.5687	34.57	0.3277	15.20	0.6389	0.4362	63.93	0.5448	21.68	0.7795	0.2399	45.39	0.3648
AutoDIR [19]	11.67	0.4697	0.6114	31.65	0.3766	15.41	0.5834	0.5079	59.65	0.5552	-	-	-	-	-
InstructIR [13]	10.92	0.3972	0.4802	46.46	0.3475	13.75	0.3240	0.4344	64.62	0.6213	-	-	-	-	-
X-Restormer [10]	10.33	0.4376	0.6093	36.12	0.3420	15.16	0.6397	0.4339	61.18	0.5468	21.57	0.7813	0.2504	46.04	0.3520
AgenticIR [65]	16.29	0.5681	0.5797	32.16	0.3762	14.26	0.5300	0.5692	54.13	0.5457	20.35	0.7304	0.2831	50.87	0.3964
FoundIR [26]	11.57	0.5220	0.4708	41.68	0.3570	15.11	0.6411	0.4296	64.18	0.5550	21.57	0.7794	0.2407	45.72	0.3554
Ours	18.57	0.6083	0.2419	44.29	0.3312	17.90	0.5147	0.2373	67.69	0.5884	23.15	0.7062	0.2538	60.15	0.4496
Methods	UHD-LL (LHD Enhancement) [25]					FoundIR-L (Low-light Enhancement) [26]					FoundIR-L+N (Joint Denoising and Enhancement) [26]				
	PSNR ↑	SSIM ↑	LPIPS ↓	MUSIQ ↑	CLIPQA+ ↑	PSNR ↑	SSIM ↑	LPIPS ↓	MUSIQ ↑	CLIPQA+ ↑	PSNR ↑	SSIM ↑	LPIPS ↓	MUSIQ ↑	CLIPQA+ ↑
PromptIR [40]	11.76	0.6170	0.4554	28.24	0.2075	16.33	0.6371	0.4871	27.62	0.2634	10.83	0.4558	0.6791	28.13	0.2543
TransWeather [44]	12.30	0.6557	0.4978	23.01	0.2004	14.95	0.6353	0.5747	22.31	0.2021	11.56	0.5256	0.6969	23.57	0.2081
DA-CLIP [36]	18.51	0.8120	0.4130	23.45	0.2807	17.34	0.7508	0.5067	25.75	0.2849	15.70	0.6457	0.6563	24.27	0.2978
DiffUIR [64]	11.27	0.5975	0.4485	26.07	0.2255	14.02	0.7172	0.3070	47.66	0.3838	13.88	0.6394	0.4514	45.58	0.3858
AutoDIR [19]	22.52	0.8572	0.3919	21.59	0.2453	21.91	0.8385	0.3563	31.55	0.3364	17.50	0.7007	0.5023	30.18	0.2821
InstructIR [13]	20.03	0.7356	0.4192	34.21	0.2324	20.04	0.8665	0.2660	47.83	0.3109	16.73	0.4719	0.6228	33.05	0.2197
X-Restormer [10]	11.56	0.6113	0.4788	26.13	0.2116	16.02	0.6432	0.5034	27.48	0.2506	9.75	0.3925	0.7185	27.62	0.2396
AgenticIR [65]	12.82	0.6649	0.4961	24.07	0.2208	8.51	0.3816	0.5595	28.09	0.2754	10.73	0.5103	0.6917	27.40	0.2696
FoundIR [26]	10.61	0.5775	0.3692	32.91	0.2394	18.98	0.8372	0.2739	49.00	0.3567	16.12	0.7272	0.4003	50.86	0.4552
Ours	20.08	0.8484	0.2334	45.24	0.3575	19.72	0.8494	0.1714	56.43	0.4009	19.72	0.7425	0.2652	61.33	0.4762
Methods	RealPhoto60 (Super-Resolution) [58]					RealDeg (Old Photo Restoration) [8]					RealDeg (Face Restoration) [8]				
	MUSIQ ↑	CLIPQA+ ↑	PIQE ↓	MANIQA ↑	PaQ-2-PiQ ↑	MUSIQ ↑	CLIPQA+ ↑	PIQE ↓	MANIQA ↑	PaQ-2-PiQ ↑	MUSIQ ↑	CLIPQA+ ↑	PIQE ↓	MANIQA ↑	PaQ-2-PiQ ↑
Real-ESRGAN [49]	59.29	0.4398	25.0258	0.5046	69.0438	54.51	0.3700	22.5213	0.4972	67.8305	51.66	0.2947	26.2679	0.4541	69.5341
BSRGAN [48]	45.46	0.3397	-	0.3759	63.3800	40.59	0.2956	35.5768	0.4008	63.9088	53.19	0.3429	26.8261	0.4486	70.0197
StabSR [61]	52.65	0.3916	27.1920	0.4361	64.3983	-	-	-	-	-	-	-	-	-	-
PASD [55]	63.53	0.4787	29.2662	0.5194	69.9744	34.59	0.2386	45.7651	0.3990	61.4419	36.97	0.2479	62.6459	0.3913	61.5455
SeeSR [51]	71.74	0.5956	26.7787	0.6077	73.8402	59.52	0.3596	29.1688	0.5115	69.9719	56.58	0.3489	28.5668	0.4509	70.5475
DreamClear [2]	70.46	0.5273	26.0232	0.6080	75.8422	52.69	0.4024	24.6792	0.5259	68.6876	54.23	0.3385	21.5950	0.4849	69.3709
OSDiff [50]	70.46	0.5725	28.6904	0.5892	73.4461	-	-	-	-	-	-	-	-	-	-
SUPIR [58]	70.26	0.5527	23.2780	0.6064	74.4188	53.30	0.3152	18.8356	0.5313	69.9300	53.17	0.3179	20.6981	0.4823	69.6014
FaithDiff [8]	72.74	0.5933	25.0027	0.6430	75.2664	53.32	0.3420	19.1189	0.5452	70.1377	59.95	0.3497	20.3812	0.5216	71.8938
Ours	72.36	0.5977	23.2547	0.6441	75.0014	62.72	0.4730	33.3370	0.5928	71.9529	64.03	0.4460	21.7626	0.5481	71.7996

capabilities in complex and diverse scenarios. Furthermore, compared with other real-world SR methods, our model also achieves significant improvements in terms of non-reference perceptual evaluations. We further present several visual comparison results in Figure 4. It can be clearly observed that the results of other methods still exhibit noticeable degradation, whereas our method performs better at simultaneously removing degradation and restoring details.

Comparison with image restoration agent. We also compare our approach with the recent image restoration agent, *e.g.*, AgenticIR [65]. Compared with AgenticIR that intelligently schedules multiple specialized restoration models, our FoundIR-v2 achieves better reconstruction quality, especially in coupled degradation tasks (Table 1 and Figure 4).

Comparison with commercial methods. We further compare our method with two popular commercial large-scale models, *i.e.*, GPT-5 and HYPIR [30]. To investigate the potential of these models when applied to challenging tasks involving unknown and complex degradations, we conduct

experiments on the mural restoration task, where the degradations are often highly uncertain and heterogeneous [43]. As presented in Figure 5, GPT-5 struggles to maintain pixel-level structural fidelity, and the generated content exhibits noticeable deviations from the original mural style. Furthermore, the recovery results of HYPIR still contain some undesirable noise. In contrast, our method produces faithful and visually pleasing results, demonstrating the generalization ability of FoundIR-v2 on unknown challenging tasks.

4.3. Ablation analysis and discussion

In this section, we conduct extensive ablation studies. Due to considerations of training costs, we select four representative sub-tasks (*i.e.*, deblurring, dehazing, low-light enhancement, and SR) for all-in-one performance analysis.

Effect of data mixture proportion. To analyze the effect of different data mixing proportions in the training batch, we train models with varying proportions under the same settings for fair comparisons. Figure 1 demonstrates that



Figure 4. Visual comparison of image restoration results on the FoundIR-L+N and RealPhoto60 benchmarks. Zoom in for a better view.

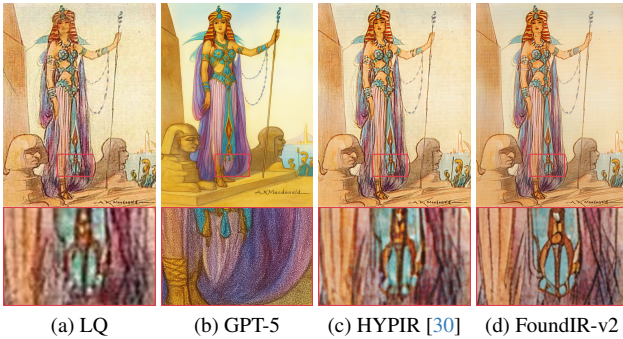


Figure 5. Visual comparison of mural restoration results.

training with equal data proportions does not yield optimal performance, as different tasks exhibit varying levels of learning difficulty. These results provide valuable insights into the training of image restoration foundation models, highlighting the importance of optimizing data mixture.

Effect of different training strategies on the same model.

We compare our data equilibrium scheduling (DES) strategy with other all-in-one training approaches, including (1) mixed training [40], (2) multi-task sequential learning [24], and (3) multi-task incremental learning [26]. Table 2 reports the average quantitative results of different variants across the four sub-tasks. Note that we retrain all comparison models for a fair comparison. We can observe that for FoundIR-v2 as a fixed model, our DES strategy achieves the best performance, outperforming other training strategies.

Furthermore, we apply our proposed DES strategy to existing all-in-one restoration models, *i.e.*, PromptIR [40]

Table 2. Ablation analysis on different all-in-one image restoration models under different training strategies. “Our*” indicates that our FoundIR-v2 is trained without the SR task for a fair comparison, since PromptIR and FoundIR do not include the SR task.

Base Models	Training Strategy				Metrics	
	Mixing	Sequence	Incremental	DES (Ours)	PSNR \uparrow	SSIM \uparrow
PromptIR [40]	✓	✗	✗	✗	15.89	0.6314
	✗	✗	✗	✓	16.92	0.6888
FoundIR [26]	✗	✗	✓	✗	16.77	0.6880
	✗	✗	✗	✓	17.95	0.7312
Ours*	✗	✗	✗	✓	20.09	0.7447
	✓	✗	✗	✗	18.91	0.6759
Ours	✗	✓	✗	✗	18.69	0.6476
	✗	✗	✓	✗	19.93	0.6725
	✗	✗	✗	✓	20.41	0.6977

and FoundIR [26]. Compared with their respective original fixed-ratio training schemes, our method brings performance gains by dynamically optimizing data mixture.

Effect of different models on the same training strategy.

To disentangle the interplay between the effectiveness of training strategies and that of models, we further analyze the effect of different models under the same training strategy. Under the same DES strategy, our FoundIR-v2 achieves a significant performance improvement over FoundIR. This confirms that, compared with FoundIR’s diffusion model learned in image space, our FoundIR-v2 leverages diffusion priors in latent space to better facilitate image restoration.

Effectiveness of MoE-driven diffusion scheduler. To validate the effectiveness of our proposed MoE-driven diffusion scheduler, we compare our architecture with other variants, including (i) without scheduler (*i.e.*, only SDXL), and

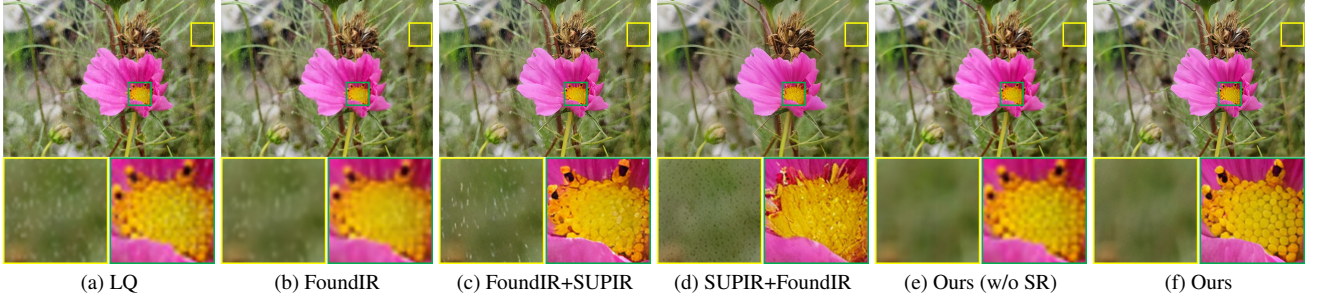


Figure 6. Visual comparison results for low-resolution image restoration. Compared to the cascaded use of FoundIR [26] (all-in-one model w/o SR task) and SUPIR [58] (SR), our FoundIR-v2 integrates both degradation removal and detail generation capabilities simultaneously.

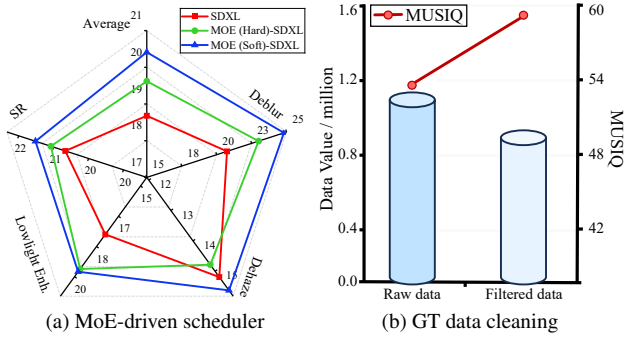


Figure 7. Statistical ablation analysis for the MoE-driven diffusion scheduler and GT data cleaning.

(ii) hard MOE-based scheduler [59] (*i.e.*, only top- k expert). We present the radar chart in Figure 7(a) to illustrate the restoration capabilities of different variants across multiple tasks. It can be observed that our designed scheduler with the soft MoE consistently obtains higher performance, as the soft gating mechanism enables adaptive collaboration among experts for better all-in-one image restoration.

Effectiveness of GT data cleaning. To demonstrate the effectiveness of GT data cleaning, we compare our approach with directly combining all datasets for training foundation model. As evidenced by the results in Figure 7(b), filtering out low-quality data from the original all-in-one training dataset can further improve the restoration performance. This also highlights that the quality of GTs is equally important for image restoration foundation model.

Discussion with other potential foundation models. We note that different universal restoration models cover different ranges of tasks. For example, for low-resolution rainy image, FoundIR [26] can perform deraining but lacks SR ability, whereas SUPIR [58] can perform SR but does not handle deraining. Compared with these all-in-one or universal restoration methods, our approach consolidates more restoration capabilities into a unified foundation model. We present an example in Figure 6. In contrast to cascadingly applying FoundIR [26] and SUPIR [58], our model produces more visually appealing results by performing rain removal and SR simultaneously. This further demonstrates that our method better leverages the synergy among different tasks.

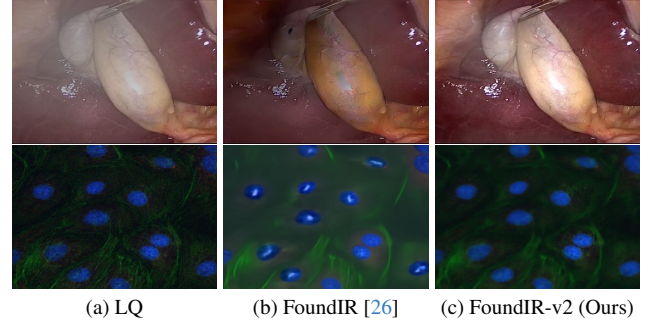


Figure 8. Visual comparison of fine-tuning the image restoration foundation models on downstream restoration tasks (laparoscopic surgery and biological microscopy image restoration).

Applications on downstream tasks. In fact, a well-trained image restoration foundation model serves as a versatile basis that can be fine-tuned for various downstream restoration tasks related to its pre-training objective. To demonstrate the applicability of image restoration foundation models to downstream tasks, we extend FoundIR [26] and FoundIR-v2 to laparoscopic surgery and biological microscopy image restoration. Since the training dataset in these tasks are typically limited and protected by privacy constraints, we fine-tune the pre-trained foundation models using only using a small amount of available data. The qualitative comparison results are provided in Figure 8. Compared with FoundIR, our FoundIR-v2 achieves better reconstruction results on these downstream tasks, highlighting the significance of developing effective image restoration foundation models.

5. Conclusion

We have presented an effective image restoration foundation model, named FoundIR-v2. We formulate a data equilibrium scheduling paradigm that dynamically optimizes all-in-one training data distributions to improve multi-task image restoration performance. Furthermore, we integrate an MoE-driven scheduler into generative pre-training to better unleash task-adaptive diffusion priors for universal image restoration. Extensive experiments and ablation analysis reveal the value of optimizing data mixture, and demonstrate the effectiveness of the proposed method.

References

- [1] Eirikur Agustsson and Radu Timofte. Ntire 2017 challenge on single image super-resolution: Dataset and study. In *CVPRW*, 2017. 5
- [2] Yang Ai, Xiaoqiang Zhou, Huaibo Huang, Xiaotian Han, Zhengyu Chen, Quanzeng You, and Hongxia Yang. Dream-clear: High-capacity real-world image restoration with privacy-safe dataset curation. *NeurIPS*, 2024. 5, 6, 7
- [3] Codruta O Ancuti, Cosmin Ancuti, Mateu Sbert, and Radu Timofte. Dense-haze: A benchmark for image dehazing with dense-haze and haze-free images. In *ICIP*, 2019. 5, 6
- [4] Codruta O Ancuti, Cosmin Ancuti, and Radu Timofte. Nh-haze: An image dehazing benchmark with non-homogeneous hazy and haze-free images. In *CVPRW*, 2020. 5, 6
- [5] Shuo Cao, Yihao Liu, Wenlong Zhang, Yu Qiao, and Chao Dong. Grids: Grouped multiple-degradation restoration with image degradation similarity. In *ECCV*, 2024. 1
- [6] Wenhui Chang, Hongming Chen, Xin He, Xiang Chen, and Liangduo Shen. Uav-rain1k: A benchmark for raindrop removal from uav aerial imagery. In *CVPRW*, 2024. 5, 6
- [7] Hanting Chen, Yunhe Wang, Tianyu Guo, Chang Xu, Yiping Deng, Zhenhua Liu, Siwei Ma, Chunjing Xu, Chao Xu, and Wen Gao. Pre-trained image processing transformer. In *CVPR*, 2021. 2
- [8] Junyang Chen, Jinshan Pan, and Jiangxin Dong. Faithdiff: Unleashing diffusion priors for faithful image super-resolution. In *CVPR*, 2025. 2, 3, 5, 6, 7
- [9] Xiang Chen, Hao Li, Mingqiang Li, and Jinshan Pan. Learning a sparse transformer network for effective image deraining. In *CVPR*, pages 5896–5905, 2023. 5
- [10] Xiangyu Chen, Zheyuan Li, Yuandong Pu, Yihao Liu, Jiantao Zhou, Yu Qiao, and Chao Dong. A comparative study of image restoration networks for general backbone network design. In *ECCV*, 2024. 5, 6
- [11] Xiangyu Chen, Yihao Liu, Yuandong Pu, Wenlong Zhang, Jiantao Zhou, Yu Qiao, and Chao Dong. Learning a low-level vision generalist via visual task prompt. In *ACM MM*, 2024. 2
- [12] Xiang Chen, Jinshan Pan, Jiangxin Dong, and Jinhui Tang. Towards unified deep image deraining: A survey and a new benchmark. *IEEE TPAMI*, 2025. 5
- [13] Marcos V Conde, Gregor Geigle, and Radu Timofte. Instructor: High-quality image restoration following human instructions. In *ECCV*, 2024. 5, 6, 7
- [14] Senyou Deng, Wenqi Ren, Yanyang Yan, Tao Wang, Fenglong Song, and Xiaochun Cao. Multi-scale separable network for ultra-high-definition video deblurring. In *ICCV*, 2021. 5, 6
- [15] Shuhang Gu, Andreas Lugmayr, Martin Danelljan, Manuel Fritsche, Julien Lamour, and Radu Timofte. Div8k: Diverse 8k resolution image dataset. In *ICCVW*, 2019. 5
- [16] Qiyuan Guan, Xiang Chen, Guiyue Jin, Jiyu Jin, Shumin Fan, Tianyu Song, and Jinshan Pan. Rethinking nighttime image deraining via learnable color space transformation. *NeurIPS*, 2025. 5, 6
- [17] Qiyuan Guan, Qianfeng Yang, Xiang Chen, Tianyu Song, Guiyue Jin, and Jiyu Jin. Weatherbench: A real-world benchmark dataset for all-in-one adverse weather image restoration. In *ACM MM*, 2025. 5, 6
- [18] Jonathan Ho and Tim Salimans. Classifier-free diffusion guidance. *arXiv preprint arXiv:2207.12598*, 2022. 5
- [19] Yitong Jiang, Zhaoyang Zhang, Tianfan Xue, and Jinwei Gu. Autodir: Automatic all-in-one image restoration with latent diffusion. In *ECCV*, 2024. 5, 6, 7
- [20] Tero Karras, Samuli Laine, and Timo Aila. A style-based generator architecture for generative adversarial networks. In *CVPR*, 2019. 5
- [21] Tero Karras, Miika Aittala, Timo Aila, and Samuli Laine. Elucidating the design space of diffusion-based generative models. *NeurIPS*, 2022. 5
- [22] Junjie Ke, Qifei Wang, Yilin Wang, Peyman Milanfar, and Feng Yang. Musiq: Multi-scale image quality transformer. In *ICCV*, 2021. 5
- [23] Diederik P Kingma and Max Welling. Auto-encoding variational bayes. In *ICLR*, 2014. 3
- [24] Xiangtao Kong, Chao Dong, and Lei Zhang. Towards effective multiple-in-one image restoration: A sequential and prompt learning strategy. *arXiv preprint arXiv:2401.03379*, 2024. 7
- [25] Chongyi Li, Chun-Le Guo, Man Zhou, Zhixin Liang, Shangchen Zhou, Ruicheng Feng, and Chen Change Loy. Embedding fourier for ultra-high-definition low-light image enhancement. In *ICLR*, 2023. 5, 6
- [26] Hao Li, Xiang Chen, Jiangxin Dong, Jinhui Tang, and Jinshan Pan. Foundir: Unleashing million-scale training data to advance foundation models for image restoration. In *ICCV*, 2025. 1, 2, 3, 4, 5, 6, 7, 8
- [27] Yawei Li, Kai Zhang, Jingyun Liang, Jiezhang Cao, Ce Liu, Rui Gong, Yulun Zhang, Hao Tang, Yun Liu, Denis Deman-dolx, et al. Lsdir: A large scale dataset for image restoration. In *CVPR*, 2023.
- [28] Bee Lim, Sanghyun Son, Heewon Kim, Seungjun Nah, and Kyoung Mu Lee. Enhanced deep residual networks for single image super-resolution. In *CVPRW*, pages 136–144, 2017. 5
- [29] Xinqi Lin, Jingwen He, Ziyang Chen, Zhaoyang Lyu, Bo Dai, Fanghua Yu, Yu Qiao, Wanli Ouyang, and Chao Dong. Diffbir: Toward blind image restoration with generative diffusion prior. In *ECCV*, 2024. 2
- [30] Xinqi Lin, Fanghua Yu, Jinfan Hu, Zhiyuan You, Wu Shi, Jimmy S Ren, Jinjin Gu, and Chao Dong. Harnessing diffusion-yielded score priors for image restoration. *arXiv preprint arXiv:2507.20590*, 2025. 2, 6, 7
- [31] Haotian Liu, Chunyuan Li, Qingyang Wu, and Yong Jae Lee. Visual instruction tuning. *NeurIPS*, 2023. 3
- [32] Ilya Loshchilov and Frank Hutter. Sgdr: Stochastic gradient descent with warm restarts. In *ICLR*, 2017. 5
- [33] Ilya Loshchilov and Frank Hutter. Decoupled weight decay regularization. In *ICLR*, 2019. 5
- [34] Xin Lu, Xueyang Fu, Jie Xiao, Zihao Fan, Yurui Zhu, and Zheng-Jun Zha. Elucidating and endowing the diffusion training paradigm for general image restoration. *arXiv preprint arXiv:2506.21722*, 2025. 2

- [35] Ziwei Luo, Fredrik K Gustafsson, Zheng Zhao, Jens Sjölund, and Thomas B Schön. Image restoration with mean-reverting stochastic differential equations. In *ICML*, 2023. 2
- [36] Ziwei Luo, Fredrik K Gustafsson, Zheng Zhao, Jens Sjölund, and Thomas B Schön. Controlling vision-language models for universal image restoration. In *ICLR*, 2024. 4, 5, 6, 7
- [37] Chenlin Ming, Chendi Qu, Mengzhang Cai, Qizhi Pei, Zhuoshi Pan, Yu Li, Xiaoming Duan, Lijun Wu, and Conghui He. Ideal: Data equilibrium adaptation for multi-capability language model alignment. *arXiv preprint arXiv:2505.12762*, 2025. 2, 3
- [38] Jin Ning, Lianbin Xie, Jie Yin, and Yiguang Liu. Cloud removal advances: A comprehensive review and analysis for optical remote sensing images. *IEEE JSTARS*, 2025. 5, 6
- [39] Dustin Podell, Zion English, Kyle Lacey, Andreas Blattmann, Tim Dockhorn, Jonas Müller, Joe Penna, and Robin Rombach. Sdxl: Improving latent diffusion models for high-resolution image synthesis. In *ICLR*, 2024. 3
- [40] Vaishnav Potlapalli, Syed Waqas Zamir, Salman H Khan, and Fahad Shahbaz Khan. Promptir: Prompting for all-in-one image restoration. *NeurIPS*, 2024. 5, 6, 7
- [41] Yuandong Pu, Le Zhuo, Kaiwen Zhu, Liangbin Xie, Wenlong Zhang, Xiangyu Chen, Peng Gao, Yu Qiao, Chao Dong, and Yihao Liu. Lumina-omnilv: A unified multimodal framework for general low-level vision. *arXiv preprint arXiv:2504.04903*, 2025. 2
- [42] Sudarshan Rajagopalan, Nithin Gopalakrishnan Nair, Jay N Paranjape, and Vishal M Patel. Gendeg: Diffusion-based degradation synthesis for generalizable all-in-one image restoration. In *CVPR*, 2025. 1, 2
- [43] Huiyang Shao, Qianqian Xu, Peisong Wen, Peifeng Gao, Zhiyong Yang, and Qingming Huang. Building bridge across the time: Disruption and restoration of murals in the wild. In *ICCV*, 2023. 6
- [44] Jeya Maria Jose Valanarasu, Rajeev Yasarla, and Vishal M Patel. Transweather: Transformer-based restoration of images degraded by adverse weather conditions. In *CVPR*, 2022. 5, 6
- [45] Ashish Vaswani, Noam Shazeer, Niki Parmar, Jakob Uszkoreit, Llion Jones, Aidan N Gomez, Łukasz Kaiser, and Illia Polosukhin. Attention is all you need. *NeurIPS*, 2017. 5
- [46] Narasimhan Venkatanath, D Praneeth, S Channappayya Sumohana, S Medasani Swarup, et al. Blind image quality evaluation using perception based features. In *NCC*, 2015. 5
- [47] Jianyi Wang, Kelvin CK Chan, and Chen Change Loy. Exploring clip for assessing the look and feel of images. In *AAAI*, 2023. 5
- [48] Jianyi Wang, Zongsheng Yue, Shangchen Zhou, Kelvin CK Chan, and Chen Change Loy. Exploiting diffusion prior for real-world image super-resolution. *IJCV*, 2024. 5, 6, 7
- [49] Xintao Wang, Liangbin Xie, Chao Dong, and Ying Shan. Real-esrgan: Training real-world blind super-resolution with pure synthetic data. In *CVPR*, 2021. 5, 6, 7
- [50] Rongyuan Wu, Lingchen Sun, Zhiyuan Ma, and Lei Zhang. One-step effective diffusion network for real-world image super-resolution. In *NeurIPS*, 2024. 5, 6, 7
- [51] Rongyuan Wu, Tao Yang, Lingchen Sun, Zhengqiang Zhang, Shuai Li, and Lei Zhang. Seesr: Towards semantics-aware real-world image super-resolution. In *CVPR*, 2024. 5, 6, 7
- [52] Jun Xu, Hui Li, Zhetong Liang, David Zhang, and Lei Zhang. Real-world noisy image denoising: A new benchmark. *arXiv preprint arXiv:1804.02603*, 2018. 5, 6
- [53] Lihe Yang, Bingyi Kang, Zilong Huang, Xiaogang Xu, Jiashi Feng, and Hengshuang Zhao. Depth anything: Unleashing the power of large-scale unlabeled data. In *CVPR*, 2024. 1
- [54] Sidi Yang, Tianhe Wu, Shuwei Shi, Shanshan Lao, Yuan Gong, Mingdeng Cao, Jiahao Wang, and Yujiu Yang. Maniqa: Multi-dimension attention network for no-reference image quality assessment. In *CVPR*, 2022. 5
- [55] Tao Yang, Rongyuan Wu, Peiran Ren, Xuansong Xie, and Lei Zhang. Pixel-aware stable diffusion for realistic image super-resolution and personalized stylization. In *ECCV*, 2024. 5, 6, 7
- [56] Zhenqiang Ying, Haoran Niu, Praful Gupta, Dhruv Mahajan, Deepti Ghadiyaram, and Alan Bovik. From patches to pictures (paq-2-piq): Mapping the perceptual space of picture quality. In *CVPR*, 2020. 5
- [57] Zhiyuan You, Zheyuan Li, Jinjin Gu, Zhenfei Yin, Tianfan Xue, and Chao Dong. Depicting beyond scores: Advancing image quality assessment through multi-modal language models. In *ECCV*, 2024. 5
- [58] Fanghua Yu, Jinjin Gu, Zheyuan Li, Jinfan Hu, Xiangtao Kong, Xintao Wang, Jingwen He, Yu Qiao, and Chao Dong. Scaling up to excellence: Practicing model scaling for photo-realistic image restoration in the wild. In *CVPR*, 2024. 2, 5, 6, 7, 8
- [59] Eduard Zamfir, Zongwei Wu, Nancy Mehta, Yuedong Tan, Danda Pani Paudel, Yulun Zhang, and Radu Timofte. Complexity experts are task-discriminative learners for any image restoration. In *CVPR*, 2025. 8
- [60] Syed Waqas Zamir, Aditya Arora, Salman Khan, Munawar Hayat, Fahad Shahbaz Khan, and Ming-Hsuan Yang. Restormer: Efficient transformer for high-resolution image restoration. In *CVPR*, 2022. 5
- [61] Kai Zhang, Jingyun Liang, Luc Van Gool, and Radu Timofte. Designing a practical degradation model for deep blind image super-resolution. In *ICCV*, 2021. 5, 6
- [62] Kaihao Zhang, Tao Wang, Wenhan Luo, Wenqi Ren, Björn Stenger, Wei Liu, Hongdong Li, and Ming-Hsuan Yang. Mc-blur: A comprehensive benchmark for image deblurring. *IEEE TCSVT*, 2023. 5, 6
- [63] Richard Zhang, Phillip Isola, Alexei A Efros, Eli Shechtman, and Oliver Wang. The unreasonable effectiveness of deep features as a perceptual metric. In *CVPR*, 2018. 5
- [64] Dian Zheng, Xiao-Ming Wu, Shuzhou Yang, Jian Zhang, Jian-Fang Hu, and Wei-Shi Zheng. Selective hourglass mapping for universal image restoration based on diffusion model. In *CVPR*, 2024. 2, 4, 5, 6, 7
- [65] Kaiwen Zhu, Jinjin Gu, Zhiyuan You, Yu Qiao, and Chao Dong. An intelligent agentic system for complex image restoration problems. In *ICLR*, 2025. 6, 7